Advanced Steel Construction – Vol. 18 No. 4 (2022) 763–772
DOI: 10.18057/IJASC.2022.18.4.4

PERFORMANCE EVALUATION OF INNOVATIVE COCONUT PALM STEM SHAPED STUD SHEAR CONNECTOR FOR COMPOSITE STRUCTURES

Rahul Tarachand Pardeshi [1, *] and Yogesh Deoram Patil [2]

[1] *Research Scholar, Sardar Vallabhbhai National Institute of Technology, Surat, India*
[2] *Associate Professor, Sardar Vallabhbhai National Institute of Technology, Surat, India*
** (Corresponding author: E-mail: rahultpardeshi@gmail.com)*

ABSTRACT

Headed studs are the more frequently employable shear connectors in composite structures. Despite its prevalence, this connector has exhibited remarkable drawbacks, prominently the shear failure at the bottom of the shank. In this research, three novel coconut palm stem (CPS) shaped studs are proposed for composite constructions, aiming to improve the shear capacity and slip performance of the connection. The traditional circular headed stud (CHS) geometry has been restructured to a proposed CPS-shaped stud while maintaining total steel material volume to be the same. Pushout tests were experimentally performed on CHS and CPS-shaped shear connectors to investigate their performance evaluation for ultimate strength, stiffness, ductility, and failure mode. Moreover, the Abaqus/Explicit has been employed to model a pushout specimen. A proposed finite element model was successfully validated with the test results for further parametric analysis. Two distinct grades of concrete and three CPS shapes were considered for the parametric investigation. Finally, three formulas were developed and proposed to predict the shear capacity of the CPS-shaped stud. The performance of the CHS and CPS-shaped stud connections was compared, revealing that the proposed CPS-shaped studs offer 37 to 47% higher shear strength, double stiffness, and slip with better ductility. So, CPS-shaped stud may substitute the traditional headed stud shear connectors in steel-concrete composite structures with added strength, stiffness, and ductility.

ARTICLE HISTORY

Received: 8 March 2022
Revised: 13 May 2022
Accepted: 14 May 2022

KEYWORDS

Composite structures;
Headed stud shear connectors;
Pushout test;
Concrete slab-steel beam;
CPS-shaped stud;
Abaqus

1. Introduction

An assemblies like concrete slab-steel beam composite element are an effective solution for infrastructures like buildings and bridges with substantial structural, economical, and architectural constraints. A concrete slab resists compressive forces, whereas a steel beam transmits tensile loads in composite beams (Ahn et al.[1]). However, the bond between the two components is insufficient to prevent the separation from acting as one unit. Consequently, steel-concrete interface shear connectors were introduced to create structures that unite the benefits of steel beam with reinforced concrete slabs (Viest [2]). Shear connections were shown to improve the bearing capacity of composite beams by more than half in comparison to non-composite beams of the same size (Shariati A et al.[3]). Numerous research has been done to predict their behaviour in composite beams (Mirza and Uy[4], Ding et al. [5], Spremic et al. [6]). Recent development shows the innovativeness in steel connectors like double-tube buckling-restrained braces steel connector (Yin et al.[7]), stiffened angle shear connectors (Nouri et al.[8]), the novel slip-released shear connector (Ding et al.[9]), concave shear connector (Pardeshi et al.[10]) and an innovative perforated steel-engineered cementitious composite connector (Tian et al.[11]) gaining advantages in the utilization of it in composite structures.

However, the most often utilized connecting device in composite constructions is headed stud shear connectors (see Fig. 1). The cylindrical shape of the headed stud offers shear capacity in both directions perpendicular to the shank's axis, but the small bottom circular part provides restricted shear capacity and inertia moment, necessitating the installation of a high number of studs in the composite beam which ultimately leads to uneconomical sections. To that aim, the adoption of alternative efficient connectors that offers high strength may be a viable solution for the assembly of composite connection. In this research, the traditional headed stud shape is restructured aiming to improve the shear capacity and develop the complete composite action of the composite connection by resembling the shanks' circular shape to a proposed coconut palm stem (CPS) shape to the headed stud without changing the total material volume. This connection is designed to be a convenient solution to the issues associated with the usage of the connectors described above, specifically (a) low shear capacity, (b) flexural stiffness, (c) moderate ductility, and (d) sudden failure due to the accumulation of shear stress at the connectors' shank root. In Experimental pushout tests on three types of CPS-shaped stud and two types of conventional headed studs (16 mm and 19 mm CHS) twine specimens were performed to investigate the shear capacity, failure mode, stiffness, and ductility of the composite connection. The performance of both types of connections was then compared. Validated simulations of various push test configurations having Abaqus finite element analysis software were used to appraise the effects of CPS shape and concrete compressive strength on the connection. Finally, three equations for predicting the shear capacity of CPS-shaped connections were established based on codal evaluation.

Fig. 1 Traditional headed stud shear connector

2. CPS-shaped stud shear connector

Shear connections are used in composite beams to withstand shear, bending, and tensile forces. As a result, shape, shearing area, and inertia are the most important factors to consider while ensuring the connection (Tabet-Derraz et al.[12]). Several categories of shear connectors have undergone a great deal of development and study over the last few decades (Pardeshi and Patil [13]). However, in composite construction, the headed stud is the more frequently utilized shear connector. Spite its popularity, this kind of connector has the small round geometric characteristics of the shank providing low inertia to stud bottom, which may ultimately responsible for stud failure (Xu et al.[14]) before reaching the concrete to its maximum limit. As a result, a unique connection in the form of CPS-shaped studs was developed in the current research as a simple solution to the difficulties associated with the failure of headed stud connection and to achieve complete composite action.

Three novel CPS-shaped studs for composite constructions are proposed here, as shown in Fig. 2. These connectors are designed so that the bottom 5 mm height should be used for welding the connector to the flange of the steel beam. These connectors geometry is unique and may suitable for Nelson Stud Welding's gun welding method, easy to install, and takes minimal time. The dimensions of the CPS-shaped studs are specified in Fig. 3. It is assumed that all dimensions can have a variation of ±0.5 mm. The proposed novel CPS-shaped shear connectors are of 3 types with identical heads, 24.6 mm diameter base and varying stem geometry. The head diameter was 32 mm with a depth of 9 mm.

The first type of CPS-shaped connector has a stem divided into two parts having a concave portion with a bottom diameter of 24.6 mm changing to 15 mm within a height of 25 mm, followed by a tapering section having 65 mm of length and a final diameter of 12 mm.

The second CPS-shaped shear connector's stem has three different cross-sectional profiles. A conical profile with a diameter decreasing from 24.6 mm to 14 mm for 20 mm height is followed by two cylindrical profiles with diameters 14 mm and 12 mm, and heights of 50 mm and 20 mm, respectively.

The third CPS-shaped connector was composed of a stem with four different profiles, namely convex, concave, conical, and cylindrical, in order from the base to the top. The diameter of the convex portion varies from 24.6 mm to

21.77 mm between a span of 10.33 mm. The concave portion attains a final diameter of 14mm with a length of 18.85 mm, followed by a conical portion with a final diameter of 12 mm and a height of 15.82 mm. The final cylindrical portion has 12 mm diameter and a length of 45 mm.

(a) CPS-1st (b) CPS-2nd (c) CPS-3rd

Fig. 2 CPS-shaped headed stud shear connectors

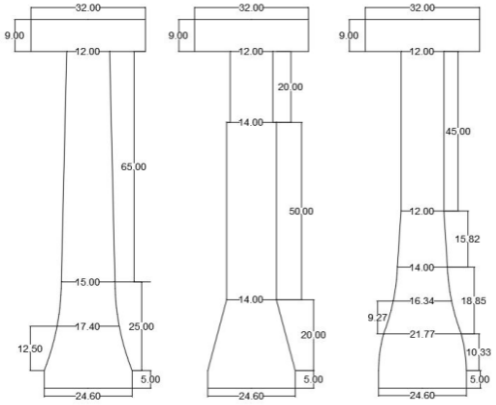

(a) CPS-1st (b) CPS-2nd (c) CPS-3rd

Fig. 3 Detailed dimensions of the CPS-shaped studs (for 16 mm average diameter)

For this research, the proposed geometry of the connection was produced in the central workshop of SVNIT, Surat as it involves cutting and chilling a standard 24.6 mm steel CHS stud into a CPS-shaped stud using lathe machine, see Fig. 4.

Fig. 4 Preparation of CPS-shaped stud using Lathe machine

3. Weld

The enlarged shank bottom area was intended to avoid stud failure at root. The root height was assume enough to guarantee adequate welding. Although the design of CPS-shaped studs allowed for gun welding, owing to its unavailability for limited volumes of research work, the fusion arc welding technique necessitated to weld the connector to the steel beam interface. The fusion arc welding was readily available in the local markets and the moderate skill labours or researchers may be able to use this method for welding.

As previously indicated, electric arc stud welding is used to weld headed studs. For arc fusion welding, E-7018 (10 No.) electrodes were used to weld the headed studs to the steel beam. In theory, the strength of a weld should, in principle, be higher than the strength of the steel plate and headed studs. However, weld quality will be impacted if welding characteristics such as electric current, lift height, and welding time are altered. As a result, weld capacity is not necessarily greater than that of steel plate and headed studs (Cao et al.[15], Cao and Shao [16]). So, the bent tests (Shim et al.[17]) as a basic laboratory test that validates the welding facts of headed studs have been used to test the weld quality (see Fig. 5). The weld was subjected to bending in an unclear way throughout the test. If an arc blow or other apparent flaw is detected, the stud must be bent such that the region to be checked inside the stress zone. Hammer blows were used to accomplish this. The studs using arc fusion welding were bent through 45° or until breakage occurs. There were no visible fractures observed in the weld and stud remain intact with weld, assuring quality of welding for further pushout testing.

(a) Arc welding (b) Hammer blow on stud (c) Initial stud (d) 45° bend stud

Fig. 5 Welding and bend test of shear connector

4. Preparation of test specimens

In the current study, ten specimens were constructed to perform the experimental pushout test. Five groups of twin specimens were considered for the average result. The CHS were used in two sets having 16 mm and 19 mm circular diameter, whereas three sets of CPS-shaped stud specimens were used for experimental testing. Table 1 describes the specimens' identity and quantity of stud material in ratio with 16 mm stud diameter. The volume of material for CPS-shaped studs was kept equal to 16 mm stud and 27% less than 19 mm stud.

Table 1
Identity of specimens with volumetric ratio

Set No.	Specimens No.	Headed Stud	The ratio of materials' volume with	
			16 mm CHS	19 mm CHS
1	1 and 2	16 mm CHS	1	0.73
2	3 and 4	19 mm CHS	1.35	1
3	5 and 6	CPS-1st	1	0.73
4	7 and 8	CPS-2nd	1	0.73
5	9 and 10	CPS-3rd	1	0.73

Moreover, the size of the steel beam does not affect the behavior of the connectors in the pushout tests (Goble and George.[18]), so the specific pushout test was performed in this study as per Eurocode 4[19] guidelines. The 200×20 mm parallel profile was used for the steel beam instead of the HEB260 profile in all specimens. The flange plate thickness of the steel beam was slightly increased to 20 mm to avoid plate buckling and to permit effective fusion arc welding of the connection in the CHS and CPS specimens against a 17.5 mm thick plate of the standard test procedure. For the preparation of parallel profile steel beam, flange plates have been welded to a 10 mm thick web plate using arc welding fusion technique. The connectors were welded to the flanges of the beams and surrounded by the concrete of the slab. It is worth noting that many researchers reduced the size of the concrete slab (Nasrollahi et al.[20], Kumar and Chaudhary[21], Kumar et al.[22]) and employed a single stud on either side of the steel beam (Kumar and Chaudhary.[21], Xue et al.[23]) for specific pushout tests. According to Anderson and Meinheit[24], the thickness of the slab does not affect the behavior and shear capacity of the connections. Therefore, in the CHS and CPS specimens, slab size was selected as 150 mm thick × 300 mm wide × 300 mm deep against the standard test, such that the bearing pressure of single centered stud on concrete during testing will not affect the strength of the connection. To prevent a splitting longitudinal fissure overhead the shear connector, Eurocode 4 [19] stipulates a minimum cover of 20 mm. So, a 25 mm cover to the reinforcement was used. All of the specimens were reinforced with 10 mm diameter rebars. On either side of the steel I-beam, two concrete slabs were placed along flange sides. The surface among the slab and the steel beam flange was lubricated so that the connection's strength will evaluate without considering the effects of surface friction. The formwork as shown in Fig. 6 was used to place the connector welded steel beam along with reinforcement mesh before pouring the concrete. After casting, the ten number of specimens as shown in Fig. 7 were ready for curing. The steel beam-concrete slab pushout

specimens were ready for testing after 28 days of water curing (see Fig. 8).

Fig. 6 Progressive preparation of specimen

Fig. 7 Ten number of specimens after concreting

Fig. 8 Ready specimens for testing

4.1. Material testing

To assess the mechanical qualities of concrete, six 150 × 300 mm cylindrical concrete specimens and three 150 × 150 mm cubes were tested under compressive and tensile forces. The average strengths of concrete in compression and tension for the form of a cylindrical specimen were 30.4 MPa and 2.4 MPa, respectively. Young's modulus was 30121.47 MPa. The standard 24.6 mm headed studs were used to fabricate the CPS-shaped connector. Local vendors supplied the standard studs. The yielding and ultimate stress, and modulus of the connector were *fy* = 450.60 MPa, *fu* = 515.90 MPa, and *Es* = 210000 MPa, respectively, and elongation of 20%. For all pushout specimens, the steel beams and reinforcing bars used 450 MPa and Fe 500 grade steel. Fig. 9a and 9b shows the stress-stain behavior of concrete and stud material, respectively.

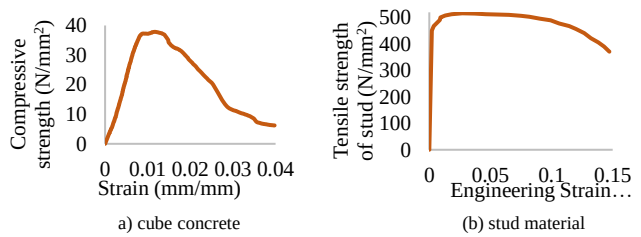

a) cube concrete (b) stud material

Fig. 9 Properties of tested materials

4.2. The portrayal of the pushout test specimens

The behavior, stiffness, and shear strength of steel beam-concrete slabs composite connections are often determined using pushout tests as per Eurocode 4 guidelines. While performing the pushout test, Eurocode 4 [19] guidelines were followed. It is recommended that specimens with CHS studs be built in a standardized design, with the dimensions of the steel beam and slab being specified in this code. On the other hand, another particular pushout test configuration is specified in the same code for specimens with different kinds of connectors. This configuration is provided without any information about the size of the pushout test components used in the setup. In this research, the specific pushout test was used to check the performance of shear connectors.

The continuous slow loading on the upper portion of the beam was applied using hydraulically loaded digital universal testing machines (UTM) (Fig. 10), generating opposite reactions to the bases of the two slabs and shear forces to the connections. UTM with a force capability of 1200 kN was utilized to perform the pushout test. The specimens were positioned beneath the UTM to verify that the weight was distributed evenly over all connectors. According to Eurocode 4 [19], successive loads were introduced slow enough on pushout specimens such that failure did not ensure in less than fifteen minutes. Digital UTM was displayed loading as "slow" on its display panel confirming 15 minutes criteria. 1000 kN capacity Load Cell having 0.04 kN least count was employed above the steel beam between two supporting plates to measure the load. The 16 mm and 19 mm CHS specimen were loaded until the stud failure. The CPS-shaped stud specimens loaded till the 20 mm maximum slip considering the observations of failure pattern/bending of connectors. The value of a slip was decided according to the FE analysis. The validated CHS studs' behavior with experimental results explained in section 8 were used to model the CPS-shaped studs.

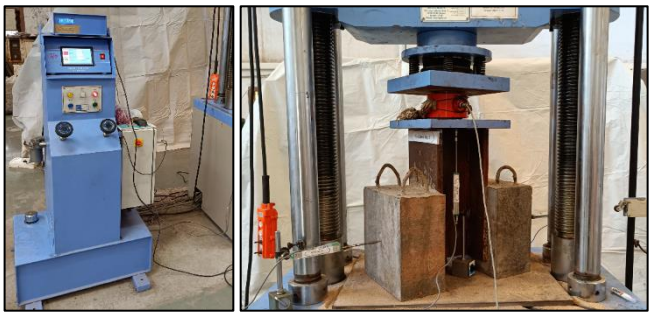

(a) Control system (b) Loading system

Fig. 10 Experimental setup

For measuring the slip among the steel beam and the concrete slab, two linear voltage differential transformers (LVDT) were used. LVDTs having 100 mm displacement capacity and 0.001 mm least count were used. In Fig.10, the various locations of the LVDT sensors on the pushout specimens are shown in more detail. Two vertical LVDTs were installed on either side of the beam web plate to measure the longitudinal slip. The data acquisition system was connected to the load cell and LVDTs for acquiring the load and longitudinal slip. In this research, the average slip was examined, and no individual data was reported.

5. Experimental findings and discussion

5.1. Load-slip performance

For the CPS-shaped connector and headed studs, the load-slip curves obtained from the pushout test are shown in Fig. 11. The average shear capacity of the 1st CPS-shaped connector was observed as 131.39 kN, compared to 95.68 kN for one 16 mm diameter CHS stud. As per Table 2, the capacity ratio of these connectors is around 1.37, indicating a 37% improvement in the CPS-shaped connector's strength over the headed stud. The average shear strength of one CPS-shaped connector for the second and third shapes was 136.92 kN and 140.59 kN. The strength ratio of the two connectors was about 1.43 and 1.47, respectively, indicating a 43% and 47% rise in the CPS-shaped connector's strength over the headed stud due to the change in geometry of the connector. It is worth noting that the shear areas ratio among the CPS-shaped stud and the CHS stud was 2.36, while the total volume was the same. This means that even though the volume of both studs is the same, the CPS-shaped studs have higher inertia at the bottom, leading to 37 to 47% more shear capacity than the CHS studs.

The average shear strength of the 1st CPS-shaped connector was observed as 131.39 kN, compared to 114.23 kN for one 19 mm diameter CHS stud. The capacity ratio of these connectors is around 1.15, indicating a 15% improvement in the CPS-shaped connector's strength over the headed stud. The strength ratio of the second and third shape connectors with 19 mm CHS stud were about 1.20

and 1.23, respectively, indicating a 20% and 23% increase in the CPS-shaped connector's strength. It is worth noting that the shear areas ratio among the CPS-shaped stud and the CHS stud was 1.67, while the total volume of the CPS-shaped stud was 27% less than the 19 mm CHS stud. This means that the CPS-shaped studs have higher inertia at the bottom, leading to 15 to 23% more shear strength than CHS stud and 27% saving in material.

The connectors are classified as ductile according to Eurocode 4 [19] if the maximum slip surpasses 6 mm. The maximum slip should measure at the 10% load fall from the ultimate strength of the connector. Based on the slip measurements, the load-slip curves (Fig. 11) reveal that all connectors showed ductile behavior. It was observed that the stiffnesses of CPS-shaped studs were 2 to 1.5 times the stiffness of 16 mm and 19 mm.

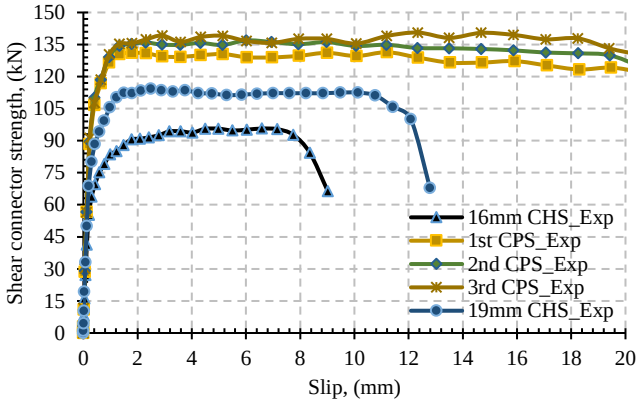

Fig. 11 Test results: Load-slip curve

5.2. Failure mode

The detected failure mechanisms of the two specimens (CHS and CPS) were different after attaining ultimate strength. The 16 mm and 19 mm CHS connectors have been sheared at the base following small deformation (see Fig. 12), whereas all CPS-shaped studs show large deflection without losing strength (See Fig. 11). The CPS-shaped studs deformed by bending away from their bottom stem and never tearing out in any location, as shown in Fig. 13. However, no failure symptoms were observed in the weld surrounding the stud base-beam flange interface. It signifies that conventional arc welding was successful in securing connection installation. The CPS-shaped studs stem bottom section was never sheared off due to a high moment of inertia at the base, whereas the headed studs failed by shear action owing to a smaller area at the base. It is reasonable to conclude that the geometric properties of studs have a great influence on the failure mode of connection.

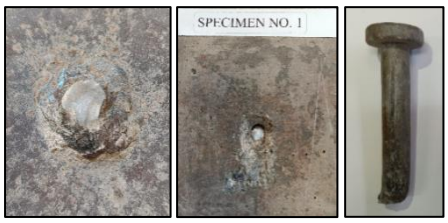

(a) specimen 1 (16 mm stud)

(b) specimen 3 (19 mm stud)

Fig. 12 Failure of headed stud shear connector

(a) CPS-1st, (b) CPS-2nd, (c) CPS-3rd

Fig. 13 Deflected shape of CPS-shaped stud

The concrete slabs were damaged in proportion to the influence of the connector deflections. In the case of CHS studs, the shearing of the CHS studs produced local concrete crushing near the connection base (see Fig. 12a), but no cracks were seen on the concrete slabs' outside surface highlighting pure stud failure without utilizing complete composite action under given concrete strength. However, in the case of a 19 mm CHS specimen, the central vertical cracks in concrete on inside edge of the slab were observed as shown in Fig. 12b, which was not the case in a 16 mm CHS specimen. For the CPS-shaped studs considering specimen no. 5, due to the multiple stresses imposed, such as the compressive forces surrounding the shank and the tensile forces beneath the stud head, the large deflection in the middle cylindrical portion of the CPS shape caused additional damage to the inside surface of a concrete slab showing composite action (see Fig. 14). External cracking was not found on the concrete slabs' outside surfaces, revealing the scope for a composite action from the concrete. However, the second CPS shape in specimen no. 8 shows small deformation of the shank in the conical portion (see Fig. 15) and more damage to the concrete in the stress zone with open cracks to the exterior surface, exhibiting complete composite action. The third CPS-shaped stud in specimen no. 9 bend in the middle of the shank due to less cross-sectional area (see Fig 16). Furthermore, cracks were discovered on the concrete slabs exterior side surface. Therefore, in conclusion, the moment of inertia and shear area at the different locations of the shank of a stud had a significant effect on connection strength-slip performance and on the failure mode. The third CPS-shaped stud showed better strength and failure performance in achieving complete composite action over the other two CPS-shaped studs.

Fig. 14 Crushing of concrete in specimen 5 (CPS-1st)

Fig. 15 Crushing of concrete in specimen 8 (CPS-2nd)

Fig. 16 Crushing of concrete in specimen 9 (CPS-3rd)

Table 2
Performance of experimentally tested shear connectors

Specimens	Stud diameter	Capacity of shear connection, P_{ult}, (kN)	Stiffness, k, (kN/mm)	(%) Rise in shear strength = $(P_{ult} - P_{16}) \times 100/P_{16}$	Maximum slip at failure, S_{fail}, (mm)	Failure observation
1 and 2	16 mm	P_{16} = 95.68	200.92	-	8.2	Stud fail in shear at the bottom of shank.
3 and 4	19 mm	114.23	299.85	19.38	11.8	
5 and 6	CPS-1st	131.39	394.18	37.32	> 20	Bending added to the middle shank and stud never failed in shear.
7 and 8	CPS-2nd	136.92	373.43	43.10	> 20	
9 and 10	CPS-3rd	140.59	385.1	46.93	> 20	

6. Establishment of finite element models and their verification with testing results

Before parametric analysis, to know the effect of the concrete strength on stud capacity, the experimental outcomes given in this work have been assessed to establish reliability to the finite element model. Abaqus (Dynamic Explicit) tool [25] was utilized to simulate the tests results of the pushout experiment. This section explains the materials model utilized in the simulations, the damage calibration, the assembly of the pushout model, the interaction details, and appropriate meshing.

Stress-strain characteristic of materials derived from testing were used to calibrate material models. Following, the model was built with accurate geometry in the assembly section. The relevant contact definitions to obtain the critical loading transfer mechanism were incorporated in the model. The following steps were performed to reduce the model's analysis run time: (1) proper symmetric boundary conditions on the planes of symmetry were determined for each half of the specimen's geometry, (2) the mesh patterns were biased substantially so that local yielding and failure at the stud base could be captured, and high-curvature surfaces could perform better when they made contact, and (3) the load was slowly applied to reduce inertial noise. The largest swept mesh length was around 25 mm for more significant convergence, while the smallest was 2 mm. In order to determine the validity of model inputs, each simulation's results were checked against the experimental data.

6.1. Material models

It is essential to characterize each component's material behavior precisely to capture the proper failure mechanisms. Material models were calibrated before building the model of the pushout specimen by representing the samples that were utilized for various tests. A similar approach of Nguyen and Kim [26] was used to establish reliable stress-strain correlations of a concrete material model, which were then included in the global model. Moreover, Pavlovic et al. [27] methodology has been adopted to calibrate the steel material properties of a tested stud for FE modeling.

6.2. Steel material models

Structural and reinforcing steel were modeled considering the bi-linear curve shown in Fig. 17. The curve depicts an elastic-plastic model. The material's tension and compression behavior were presumed to be identical. A tri-linear curve was employed to characterize the stress-strain relationship of headed studs in a global model, as represented in Fig. 18.

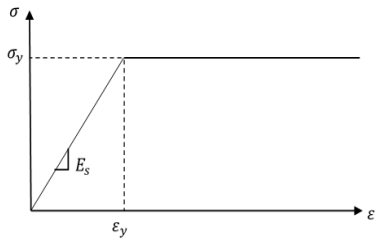

Fig. 17 Stress-strain diagram of structural and reinforcing steel for FE analysis

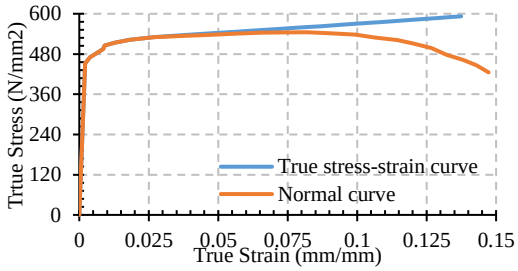

Fig. 18 Stress-strain diagram of stud material for FE analysis

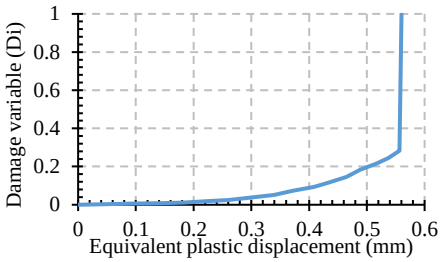

Fig. 19 Damage evolution

It is first necessary to know metal plasticity. Before fracture, the true stress-strain data is crucial for ductile fracture assessment under monotonic loading. The undeformed structure has engineering stress (s) and strain (e), whereas the smaller cross-sectional area has true stress (σ) and true strain (ε). Since the tension state becomes triaxial following necking activation, measuring true stress and strain from uniaxial tensile testing is challenging. However, the metals' real behavior may be computationally simulated for calibration following necking activation. Only stresses and strains in a triaxial stress condition must be associated. The necking activation uses equivalent stress and strain as a function of stress triaxiality (η=1/3 for uniaxial tension). Calibration data set processing of Abaqus [25] may be used to convert engineering stress and strain to true values or can calculate using relations, $\sigma_i = s_i(1 + e_i)$ and $\varepsilon_i = ln(1 + e_i)$. This study utilized isotropic plasticity, starting modulus of elasticity E = 210 GPa, and Poisson's ratio = 0.3 for the headed stud and steel segments. The tension test's nominal stress and strain curve was calibrated for true stress and strain value for headed stud material in the numerical simulation. The damage variable (Di) in consideration with equivalent plastic displacement was utilized in modeling to define the damage of post-necking material behavior as a damage evolution law as shown in Fig. 19. D=0 signifies no damage during necking activation, whereas D=1 represents maximum damage at fracture, according to the software's description [21]. For simulating necking activation, the fracture strain of the material was characterized in the FE model as an equivalent true plastic strain (ε_{up}) at the ultimate true stress state as per Rice and Tracey [28] plastic relationships and fracture law model. Here, ε_{up} = 0.338 as a function of stress triaxiality (η = -0.33 to 2) (Pavlovic et al. [27]) was calibrated for experimental results using Eq. (1). Here, β is material factor depend on void grow, usually having 1.5 value. ε_n^{pl} stain value at ultimate stress.

$$\varepsilon_{up}(\eta) = \varepsilon_n^{pl} . exp(-\beta \cdot \eta + \beta . 1/3) \quad (1)$$

It is worth noting that Abaqus [25] has the capability of removing parts that have been severely damaged. *Dmax* = 0.99 is the default threshold value. A damage element is removed from the FE model if its damage index value *D* at

each junction of two different point exceeds *Dmax*. The post-necking ductile damage evolution value was extracted using the calibrated simulation, which was then utilized in detailed parametric models for FE analysis. The fracture strain ($\varepsilon_{usp} = 0.645$) as a function of the shear stress ratio, 1.8, are the characteristics that were defined the shear damage. For a failure displacement of 2.67 mm, the evolution response was tuned to linear softening and multiplicative degradation.

6.3. Concrete material models

The Concrete Damage Plasticity (CDP) model simulated the nonlinear concrete behavior, as damage parameters can be calibrated using this model, which allows degradation of stiffness and plastic deformations to be represented [21]. Fig. 20 (a) and (b) illustrate compressive and tensile concrete stress-strain curves. The curve of concrete compression has three parts. The first section is in the elastic range of the relative limit state, $0\ to\ 0.4f_{cm}$. The nonlinear parabolic component of the curve in the second segment starts at the relative limit stress $0.4f_{cm}$ and progresses to the concrete capacity f_{cm} following nonlinear parabolic segment as per Eq. (2) (Eurocode 2[29]). The section of the curve from f_{cm} to a value of αf_{cm} is the third section.

Here, the cylindrical compressive strength of concrete, $f_{cm} = 0.8\, f_{cu}$, and f_{cu} is a cube strength in MPa. The value of strain (‰) corresponding to f_{cm} is $\varepsilon_{c1} = 0.7{f_{cm}}^{0.31}$. The initial young's modulus, E_{cm} was calculated using Eq. (3) [15]. Poisson's ratio was 0.2. Factor α = 1 or less to 0.5 referred to Eurocode 2 [29] and Ellobody et al. [30]. In this study, for a good calibration of FE results, α = 0.85 was referred from the investigation of Nguyen and Kim [26]. The third section ends at $\varepsilon_{cu} = 0.0035$ suggested by Eurocode 2 [29], but for good agreement of experimental results with FE analysis, Nguyen and Kim [26] used $\varepsilon_{cu} = 0.01$, and the same was adopted here in the detailed parametric investigation of this study.

$$f_{ci} = \left(\frac{\kappa\xi - \xi^2}{1+(\kappa-2)\xi}\right) f_{cm}, 0.4\, f_{cm} < f_{ci} < f_{cm} \tag{2}$$

Here,

$$\kappa = 1.1E_{cm} \times (\varepsilon_c / f_{cm})\ \ and\ \ \xi = \varepsilon_{ci} / \varepsilon_c, \left(\frac{0.4\, f_{cm}}{E_{cm}}\right) < \varepsilon_{ci} < \varepsilon_c \tag{3}$$

$$E_{cm}\ (Mpa) = 22 \times 10^3 \times (0.1\, f_{cm})^{0.3}$$

Concrete tensile properties refer to Eqs. (4) and (5) for two segments of the tensile curve. The first segment with a linear pattern followed E_{cm} up to the highest tensile strength, f_{ctm} as per Eq. (4) up to the cracking strain, ε_{ctr} specified by Wang and Hsu [31]. The tension stiffening segment as per Eq. (5) defines the weakening function up to the total tensile strain, ε_{ctu} in the second segment. Here, the value of ε_{ctu} was selected as 0.005 for stable post processing of FE analysis and to avoid unnecessary errors.

$$f_{ctm} = 0.3(f_{cm} - 8)^{(2/3)} \tag{4}$$

$$f_{ct} = f_{ctm}(\varepsilon_{ctr} / \varepsilon_{ct})^{0.4}, \varepsilon_{ctr} < \varepsilon_{ct} < \varepsilon_{ctu} \tag{5}$$

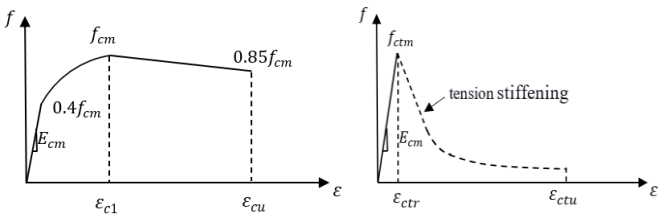

(a) compression (b) tension

Fig. 20 Stress-strain relationship of concrete material

Damaged plastic models with uniaxial material compositions were employed to pretend concrete materials' nonlinearities in compression, D_C and tension, D_t. As part of the modulus deterioration phase, the damage variables $D_C = 1 - (f_{ci}/f_{cm})$ and $D_t = 1 - (f_{ct}/f_{ctm})$ were specified. The CDP was defined by the ratio in biaxial to uniaxial state (1.16), flow potential eccentricity (0.1), deviatoric cross-section parameter (0.667), and material dilation angle (30). For verification and parametric studies, Table 3 lists the concrete properties.

Table 3
Concrete properties

Concrete properties	Grade of concrete		
	Experimental	C30	C40
f_{cm} (MPa)	30.4	38	48
ε_{c1} (‰)	2.01	2.2	2.3
f_{ctm} (MPa)	2.4	2.9	3.5
E_{cm} (GPa)	30.71	33	35

6.4. Finite element model

A pushout test was done on five different models with 16 mm, 19 mm, and three types of CPS-shaped studs. All models represent the half model geometry of test setup considering aspects of the standard pushout test with proper symmetric boundary conditions. The 16 mm and 19 mm detailed half model having CHS stud were used for comparison purposes with three different CPS-shaped studs for performance evaluation under different strength of concrete.

ABAQUS dynamic explicit was used to address the complex geometry and nonlinear FE performance of the CPS-shaped studs' pushout test specimens. Dynamic explicit is capable of dealing with complex nonlinear problems, damage, and failures. The FE analysis included geometry parts and assembly, partitions, meshing and element types, contact-interaction, boundary condition and loading, material constitutive models, damage, and failure. The preceding sections present the detailed FE models and their inclusion. A total of 10 pushout test specimens were evaluated in this investigation. Table 4 reveals the specimen identification used in research study. The CPS-shaped stud specimens have an average 16 mm stud diameter and concrete strength, 30.4MPa, 38Mpa and 48Mpa. The material properties of structural steel beam, headed stud, and reinforcement are considered identical as of testing.

The correctness of the FE analysis relies heavily on the accurate sketching of all connection components in the part module. Steel beam, reinforced concrete slab, and headed stud shear connector are the main components of the connection. Other components include reinforcing rods and a rigid base. The partition of parts has a significant impact on good meshing, so the specimen parts were partitioned to apply the proper meshing technique. The assembly module brought together all of the components that impacted the model's positioning (see Fig. 21).

A successful FE analysis relies heavily on good meshing. There are several factors that mesh components need to consider when determining stress gradients. The coarse mesh was used in the FE model to speed up the study process. Adding a fine mesh to the concrete/stud interface allowed more precise results. Fine mesh size was also employed in the headed stud at the point where the stud will fail under shear stress. The smallest mesh size was chosen to be 2 mm to better convergence, while the maximum mesh length was 25 mm. Generally, there is a specific process that most geometries can be expressed in a structured mesh. To handle complex geometries, swept meshing utilizes an internally generated mesh that is extruded or revolved around an axis of rotation. Due to the complexity of pushout test modeling and the associated difficulties with convergence, swept meshing (shown in Fig. 21) was considered for FE analysis. Along with meshing, one of the most important aspects of FE analysis is the selection of the correct element type. For plasticity, interactions, large deformations, and failure analysis, the 8-node brick (C3D8R) solid elements with reduced integration stiffness were used to mesh with the concrete slab with a geometric hole, steel beam, and the headed stud shear connector in all models. The T3D2 and R3D4 truss elements were applied to model the rigid block and rebars.

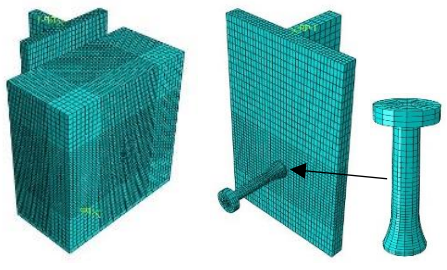

Fig. 21 Assembly and meshing of half-model

General contact and tie constraints have been used to designate the proper interaction between the assembled components. The geometric hole surface and the stud surface were tied together to eliminate relative slip between the two surfaces when using the tie constraint. The steel flange and concrete slab surfaces were typically greased when conducting experimental pushout tests to avoid friction between the two surfaces, so they were subjected to frictionless contact interaction in FE modeling. The interface of the bottom of the stud and beam flange was restrained using a tie constraint. To interpolate the nodes' translational DOF, reinforcement in concrete interacted with an embedded constrain inside the concrete slab. The concrete slab was assumed to rest on a rigid base in detailed FE models, and the surfaces have interacted with each other using contact properties. The "hard contact" and the penalty function with a friction coefficient of 0.2 were used to define the contact interaction between the rigid base and the base of the concrete slab along with normal and tangential directions. With the help of a fixed reference point and rigid body constraint, the rigid base was secured for all DOF boundary conditions. The final detailed FE models applied the z-direction symmetric boundary to the steel web's edge. To avoid a sudden change in inertia forces, the dynamic-explicit analysis generally requires a smooth loading condition. As a result, the displacement-based load was applied to the steel beam's upper area using a smooth load amplitude function of Abaqus [25] in the current analysis.

6.5. Validation

Fig. 22 depicts the theoretical load-slip curves compared with the test results to demonstrate the validity of the FE modeling. Fig. 23 describing the deflected shape of CPS-shaped studs validating the FE analysis and experimental study. No significant discrepancies were found between the experimental test curve and the FE analysis study when verifying the results for elastic and inelastic behavior of the connections. In comparison between the failure mode (fracture) of the studs in the numerical analyses and tests, Fig. 24 highlighting the fracture of stud at the root zone having equal magnitude of slip for test result (see Fig. 22). To validate FE analytical results with the experimental load-slip curve, the values of ductile and shear damage initiation, as well as the damage evolution response of steel material, were calibrated. These calibrated values have been utilized in the modeling of parametric analysis.

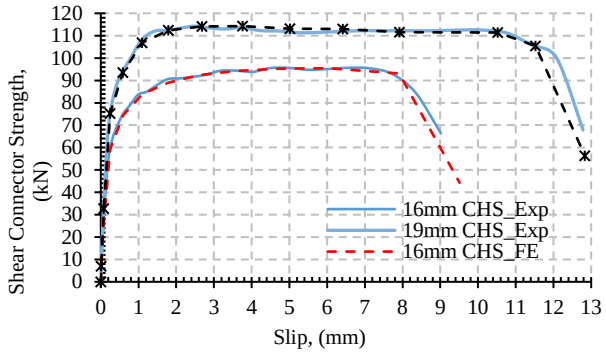

Fig. 22 Verification of FE analysis results with experimental findings

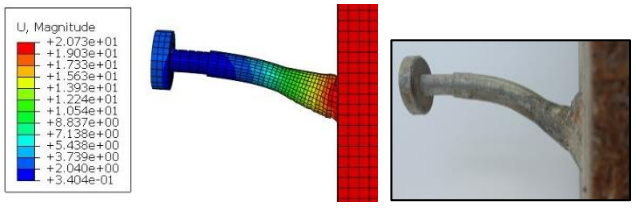

(a) Deflected shape of CPS-2nd

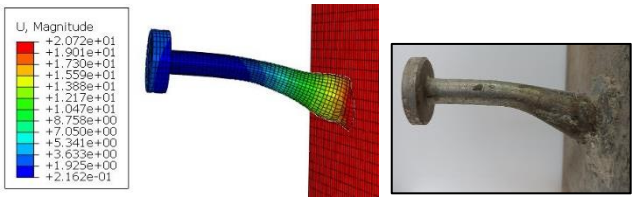

(b) Deflected shape of CPS-3rd

Fig. 23 Deflected shape of CPS-shaped stud for validation of FE analysis and experimental study

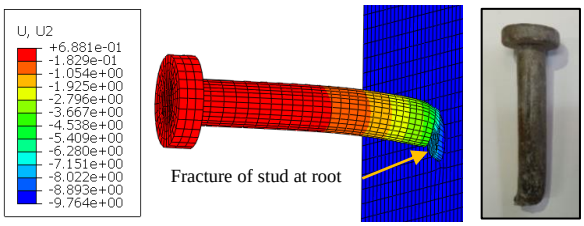

(a) for 16mm headed stud

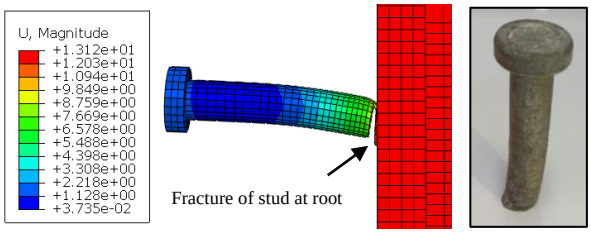

(b) for 19mm headed stud

Fig. 24 Comparison between the failure mode (fracture) of the studs in the numerical analyses and experimental tests

7. Parametric analysis results and discussions

The influence of stud shape and concrete strength on connection performance in terms of capacity, stiffness, and slip performance are discussed here. The CHS is compared to the findings of FE analysis of pushout tests on specimens with three CPS-shaped studs and two varying concrete strengths, f_{cm}, 38 and 48 N/mm^2. FE analysis revealed the ultimate load per stud (P), percentage rise in shear strength, stiffness (k), and slip at the failure of 10 pushout specimens. The entire response at the reference point acting on the top surface of a steel beam was used to compute the load. The nodes on the flange and slab at the stud center were selected to determine the connection slip. It is necessary to exercise the maximum slip capacity at failure, which is determined as per the characteristic slip given by Eurocode 4 [19]. The maximum slip capacity at failure should be exercised at 10 percent load level descends below the ultimate load as shown in Fig. 25. Following Eurocode 4 [19], the stiffness of the shear connection was estimated according to the formula, $k = 0.7P_{rk}/S_{prk}$, where P_{rk} is the characteristic load, which was taken from the load-slip curve as $0.9P$, and S_{prk} is the slip that corresponded to $0.7P_{rk}$ (see Fig. 25).

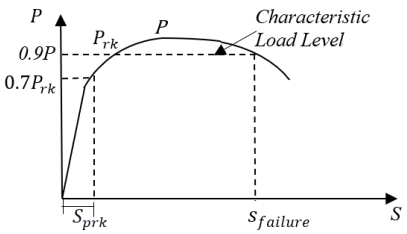

Fig. 25 Determination of stiffness and slip capacity

7.1. Effect of the strength of concrete on ductility and shear capacity of CPS-shaped shear connector

The FE model accurately signified the behavior of the shear connectors in composite beam-slabs specimen. The concrete strength is a well-known factor that influences the behavior of traditional headed studs (Ahn et al.[1], Cao et al.[15], Cao and Shao[16], Anderson and Meinheit [24]). In this parametric study, the effect of varying strength of concrete on CPS-shaped studs performance was analyzed. The FE analysis results show that the CPS-shaped studs under higher strength concrete performed well in strength and ductility than 16 mm and 19 mm CHS. The 16 mm stud was rigid under 38 and 48 N/mm^2 strength concrete (see Fig. 26a), whereas all CPS-shaped studs were ductile in behavior due to improved slip performance. Here, the shear connector is termed ductile if the ultimate slip of the connection is equal to or more than 6 mm, according to Eurocode 4 [19]. Fig. 27 compares the CHS and CPS-shaped studs' performance under C30 and C40 grade concrete. The strength of CPS-shaped studs was approximately improved up to 50 to 65% under higher grade concrete because of unique CPS geometry than 16 mm CHS. Table 4 summarizes the ultimate load per stud (P_{ult}), percentage rise in strength, stiffness (k), maximum slip at the failure, and ductility performance of 10 pushout specimens obtained

during FE studies. It was observed that the stiffnesses of CPS-shaped studs were 2 to 1.5 times more than the stiffness of 16 mm and 19 mm.

Table 4
Performance evaluation of CPS-shaped studs under varying strength of concrete

Concrete Strength, F_{cm}, (MPa)	Stud type	Capacity of shear connection, P_{ult}, (kN)	Stiffness, k, (kN/mm)	(%) Rise in shear strength = $\frac{(P_{ult}-P_{16})\times 100}{P_{16}}$	Maximum slip at failure, S_{fail}, (mm)	Ductility performance
38	16 mm CHS	101.02	212.16	0	5.8	Non-Ductile
	19 mm CHS	130.03	334.36	28.70	9.1	Ductile
	CPS-1st	151.74	413.83	50.19	16.5	Ductile
	CPS-2nd	157.03	426.42	55.43	13.7	Ductile
	CPS-3rd	155.47	416.79	53.89	16	Ductile
48	16 mm CHS	106.81	224.29	-	5	Non-Ductile
	19 mm CHS	143.38	361.32	34.24	7.2	Ductile
	CPS-1st	170.07	459.85	59.23	9.8	Ductile
	CPS-2nd	173.19	474.40	62.16	8.5	Ductile
	CPS-3rd	175.61	472.80	64.41	10.7	Ductile

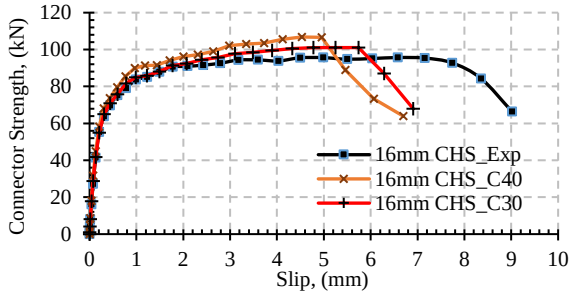

(a) 16 mm CHS load-slip curve

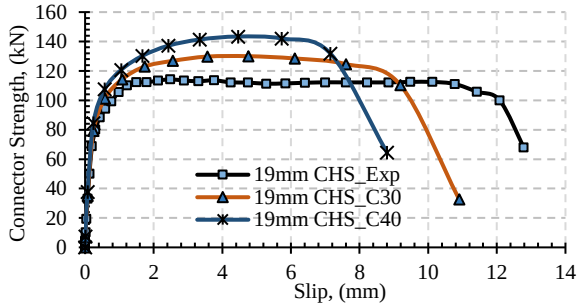

(b) 19 mm CHS load-slip curve

Fig. 26 Ductility (slip) performance of CHS under C30 and C40 grade concrete

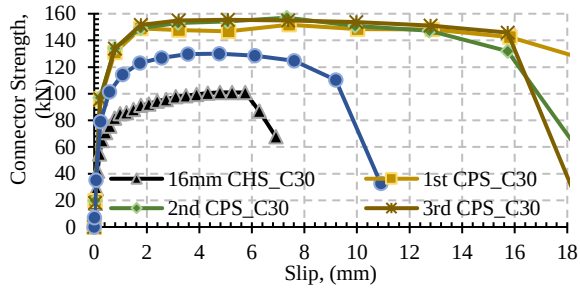

(a) Load-slip curve for C30

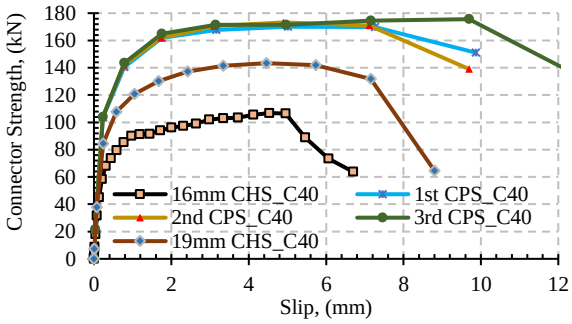

(a) Load-slip curve for C40

Fig. 27 Performance comparison for shear capacity and slip under CHS and CPS-shaped studs

7.2. Evaluation of codes for the strength of CPS-shaped connector

The experimentally evaluated shear capacity of CHS specimens under uniaxial loading is compared with the design codes' assessment findings, particularly for Eurocode4 [14], GB50017-2003 [32], AISC [33], and JSCE [34](Xu et al.[14]). The application of these standards on assessing the shear capacity of CHS studs is addressed here. Table 5 describes the capacity equation as per standard codal provisions. Here, P is the shear strength of a stud in N, h is the connector height in mm, d is the stud shank diameter in mm, and As is the area in mm^2.

Table 5
The code-based equations for calculating the headed stud shear capacity (N).

Sr. No.	Reference	Shear-capacity equations	Equation No
1	Eurocode 4 [19]	$P = 0.29\alpha d^2\sqrt{E_c f_{cm}} \le 0.8 A_s F_u$ Here, $\alpha = 0.2\left(\frac{h}{d}+1\right)$ $for\ 3 \le h/d \le 4$ $\alpha = 1$ for $h/d > 4$	(6)
2	GB50017 [32]	$P = 0.43 A_s\sqrt{E_c f_{cu}} \le 0.7 A_s F_u$	(7)
3	AISC [33],	$P = 0.5 A_s\sqrt{E_c f_{cm}} \le A_s F_u$	(8)
4	JSCE [34](Xu et al.14])	$P = 56.4 d^2\sqrt{f_{cm}}$ $(h/d \ge 5.5)$	(9)
		$P = 10.32 dh\sqrt{f_{cm}}$ $(h/d < 5.5)$	(10)

Table 6
Evaluation of codes for the strength of shear connection (kN)

Stud Type	P_{EXP}	EC 4	GB50017	AISC	JSCE	P_{EXP}/EC4	P_{EXP}/GB5	P_{EXP}/AISC	P_{EXP}/JSCE
16 mm CHS	95.68	71.73	72.57	97.08	79.60	1.33	1.31	0.98	1.20
19 mm CHS	114.23	101.15	102.33	136.90	112.43	1.12	1.11	0.83	1.01

Table 6 shows the tested stud shear capacity of 16 mm and 19 mm CHS studs and the associated design values based on various design provisions. There have been discrepancies in the specification-based evaluations. In comparison to the test findings, the AISC evaluation results are close to the stud shear capacity for 16 mm CHS; however, the JSCE (Xu et al.[14]) Eq. 10 based evaluation results are closer to the 19 mm CHS tested capacity. The difference in assessment findings of the other two specifications is approximately 11% in variation with experimental test results. AISC underestimated the effects of a larger diameter stud on shear capacity, whereas JSCE forecasted nearly equal value to 19 mm stud capacity. For the estimate of the unfactored shear strength of a connector, Eurocode 4 [19] and GB50017 [32] specifies Eq. (6) and Eq. (7) with a $0.8A_sF_u$ and $0.7A_sF_u$ constraint respectively resulting underestimated shear capacity of connector. Whereas JSCE [34](Xu et al.[14]) Eq. 10 considers the combined effect of varying concrete strength and diameter of stud for forecasting the shear capacity of connector. As a result, Eq. 10 with multiplying modification factor α are considered here, which may to forecast the stud capacity of changed designs geometry in varying concrete grade such as CPS-shaped studs with larger base diameter incorporated in different grade of concrete. The unitless modification factor, α is the ratio of capacities of CPS-shaped stud to the CHS having same larger base diameter (here the diameter of CHS is 24.6 mm), $P_{CPS}/P_{24.6}$, see Table 7. Therefore, the three formulas are proposed to calculate the shear capacity of CPS-shaped studs as follows.

Table 7
Forecasting of the modification factor, α

Code	$P_{24.6}$	$\alpha = P_{CPS}/P_{24.6}$		
		CPS-1st = 131.39 kN	CPS-2nd = 136.92 kN	CPS-3rd = 140.59 kN
Eurocode 4 [19]	169.57	0.77	0.81	0.83
GB50017[32]	171.55	0.76	0.80	0.83
AISC[33]	229.50	0.57	0.59	0.61
JSCE[34][9]	145.57	0.90	0.94	0.96

For CPS-1st, $Q = 9.29 d_b h\sqrt{f_{cm}}$ (11)

For CPS-2nd, $Q = 9.70 d_b h\sqrt{f_{cm}}$ (12)

For CPS-3rd, $Q = 9.91 d_b h\sqrt{f_{cm}}$ (13)

Here, Q is the shear capacity of the connector, d_b is the large bottom diameter of CPS-shaped stud, h is the height of the connector, and f_{cm} be the cylindrical compressive strength of concrete.

Verification of the newly presented equations (Eq. 11 to 13) to calculate the shear capacity of CPS-shaped stud under varying concrete strength is described in Table 8. The strength of CPS-shaped stud by the FE analysis and predicted value by the proposed equations are almost identical. The ratio P_{FE}/Q is in the range of 0.99 to 1.03, verifying that the application of proposed equations to CPS-shaped studs is acceptable.

Table 8
Verification of proposed formulas under varying strength of concrete

Concrete Strength, F_{cm}, (MPa)	Stud type	FE results, P_{FE}, (kN)	Predicted capacity of CPS-shaped stud, Q	P_{FE}/Q
38	CPS-1st	151.74	146.51	1.03
	CPS-2nd	157.03	152.98	1.02
	CPS-3rd	155.47	156.29	0.99
48	CPS-1st	170.07	164.66	1.03
	CPS-2nd	173.19	171.93	1.01
	CPS-3rd	175.61	175.65	1.00

8. Conclusions

New CPS-shaped shear connectors for composite structures are proposed in the present research as an alternative to the traditional headed studs. The CPS-shaped connectors are the restructured geometry of headed studs having a large bottom area and the same overall volume. Three types of CPS-shaped connectors and two traditional-headed studs were experimentally tested under pushout loading to study their shear capacity and slip performance. Whereas the effects of modifying the shape of headed studs as CPS shape and varying concrete strength on shear connections' ultimate capacity and ductility were investigated through FE analysis. From the observations of experimental and FE studies, the following conclusions have been obtained:

- In the case of CPS-shaped studs having the same volume as 16 mm headed stud, the CPS-shaped studs have 37 to 47% higher shear strength and 2 times more stiffness than CHS studs because of the increased inertia at their bottom.
- In the case of CPS-shaped studs having 27% less overall volume than 19 mm headed stud, the CPS-shaped studs offer 15 to 23% more shear strength, 1.5 times more stiffness, and 27% saving in steel material than CHS studs.
- The geometrical design of the CPS-shaped connector conferred ductile behavior to the connection; moreover, it nourished more than twice the ductility to the connection before stud failure compared to the CHS.
- The FE model accurately predicted the behavior of the shear connector and validated the experimental findings of pushout testing.
- The FE analysis results revealed that all CPS-shaped studs exhibited ductile behavior due to enhanced slip performance compared to the rigid behavior of 16 mm CHS studs under C30 to C40 grade concrete. Because of the distinctive CPS shape compared to 16 mm CHS, the strength of CPS-shaped studs was increased by 50 to 65 percent under C30 to C40 grade concrete.
- Finally, based on the FE parametric analysis and codal evaluations, three formulas for predicting the shear strength of the CPS-shaped stud were developed and proposed for composite structures.

Acknowledgement

The authors are grateful to the Ministry of Education (MoE) India, and Sardar Vallabhbhai National Institute of Technology Surat, India, for the support received.

References

[1] Ahn J.H., Kim S.H., and Jeong Y.J., "Shear behaviour of perfobond rib shear connector under static and cyclic loadings," Magazine of Concrete Research, 60(5), 347–357, 2008, doi: 10.1680/macr.2007.00046.
[2]Viest I.M., "Investigation of stud shear connectors for composite concrete and steel T-beams," ACI Journal Proceedings, 52(4), 875–892, 1956, doi: 10.14359/11655.
[3] Shariati A S.M., Sulong NHR, and Suhatril M., "Various types of shear connectors in composite structures: A review," International Journal of the Physical Sciences, 7(22), 2876–2890, 2012, doi: 10.5897/IJPSX11.004.
[4] Mirza O., and Uy B., "Effects of strain regimes on the behaviour of headed stud shear connectors for composite steel-concrete beams," Advanced Steel Construction, 6(1), 635–661, 2010.
[5] Ding Y., Dai X.M., and Yan J.B., "Developments and behaviors of slip-released novel connectors in steel-concrete composite structures," Advanced Steel Construction, 15(1), 30–36, 2019, doi: 10.18057/IJASC.2019.15.1.5.
[6] Spremic M., Markovic Z., Veljkovic M., and Budjevac D., "Push-out experiments of headed shear studs in group arrangements," Advanced Steel Construction, 9(2), 139–160, 2013, doi: 10.18057/IJASC.2013.9.2.4.
[7] Yin Z., Feng D., Yang B., and Pan C., "The seismic performance of double tube buckling restrained brace with cast steel connectors," Advanced Steel Construction, 18(1), 436-445, 2022, doi: 10.18057/IJASC.2022.18.1.2
[8] Nouri K., Sulong N.H.R., Ibrahim Z., and Shariati M., "Behaviour of novel stiffened angle shear connectors at ambient and elevated temperatures," Advanced Steel Construction, 17(1), 28-38, 2021, doi:10.18057/IJASC.2021.17.1.4.
[9] Ding Y., Dai X., and Yan J., "Developments and behaviors of slip-released novel connectors in steel-concrete composite structures," Advanced Steel Construction, 15(1), 30-36, 2019, doi: 10.18057/IJASC.2019.15.1.5 30
[10] Pardeshi R.T., Singh P.A., and Patil Y.D., "Performance assessment of innovative concave type shear connector in a composite structure subjected to push-out loading," Materials Today: Proceedings, 2022, doi:10.1016/j.matpr.2022.03.262
[11] Tian L., Liu T., Li T., and Lin H., "Shear resistance of novel perforated shaped steel-engineered cementitious composite (ECC) connectors," Advanced Steel Construction, 16(1), 30-36, 2020, doi: 10.18057/IJASC.2020.16.1.4 30
[12] Tabet-Derraz M.I., Khelil A., Hamdaoui K., Boumechra N., and Abdallah M., "Experimental and numerical study of an innovative OMEGA-shaped connector for composite beams," Structures, 32(8), 279–297, 2021, doi: 10.1016/J.ISTRUC.2021.02.050.
[13] Pardeshi R.T., and Patil Y.D., "Review of various shear connectors in composite structures," Advanced Steel Construction, 17(4), 394–402, 2021, doi: 10.18057/IJASC.2021.17.4.8.
[14] Xu C., Sugiura K., Wu C., and Su Q., "Parametrical static analysis on group studs with typical push-out tests," Journal of Constructional Steel Research, 72(6), 84–96, 2012, doi: 10.1016/J.JCSR.2011.10.029.
[15] Cao J., Shao X., Deng L., and Gan Y., "Static and fatigue behavior of short-headed studs embedded in a thin ultrahigh-performance concrete layer," Journal of Bridge Engineering, 22(5), p. 04017005, 2017, doi: 10.1061/(asce)be.1943-5592.0001031.
[16] Cao J., and Shao X., "Finite element analysis of headed studs embedded in thin UHPC," Journal of Constructional Steel Research, 161(10), 355–368, 2019, doi: 10.1016/J.JCSR.2019.03.016.
[17] Shim C.S., Lee P.G., and Yoon T.Y., "Static behavior of large stud shear connectors," Engineering Structures, 26(12), 1853–1860, 2004, doi: 10.1016/j.engstruct.2004.07.011.
[18] Goble and George. G., "Shear strength of thin flange composite specimens," Engineering Journal, American Institute of Steel Construction, 5, 62–65, 1968.
[19] Eurocode 4, Design of composite steel and concrete structures - Part 1-1: General rules and rules for buildings. London, 2004.

[20] Nasrollahi S., Maleki S., Shariati M., Marto A., and Khorami M., "Investigation of pipe shear connectors using push out test," Steel and Composite Structures, 27(5), 537–543, 2018, doi: 10.12989/scs.2018.27.5.537.
[21] Kumar P. and Chaudhary S., "Effect of reinforcement detailing on performance of composite connections with headed studs," Engineering Structures, 179(1), 476–492, 2019, doi: 10.1016/J.ENGSTRUCT.2018.05.069.
[22] Kumar P., Patnaik A., and Chaudhary S., "Effect of bond layer thickness on behaviour of steel-concrete composite connections," Engineering Structures, 177(12), 268–282, 2018, doi: 10.1016/J.ENGSTRUCT.2018.07.054.
[23] Xue W., Ding M., Wang H., and Luo Z., "Static behavior and theoretical model of stud shear connectors," Journal of Bridge Engineering, 13(6), 623–634, 2008, doi: 10.1061/(asce)1084-0702(2008)13:6(623).
[24] Anderson N.S., and Meinheit D.F., "Steel capacity of headed studs loaded in shear," RILEM Symposium on Connections Between Steel and Concrete, Illinois, USA, 202–211, 2001.
[25] ABAQUS, "Abaqus user's manual version 2019," Dassault Systèmes Simulia Corp.: Providence, RI, USA. 2019.
[26] Nguyen H.T., and Kim S.E., "Finite element modeling of push-out tests for large stud shear connectors," Journal of Constructional Steel Research, 65(10–11), 1909–1920, 2009, doi: 10.1016/J.JCSR.2009.06.010.
[27] Pavlović M., Marković Z., Veljković M., and Bucrossed D.S.D., "Bolted shear connectors vs. headed studs behaviour in push-out tests," Journal of Constructional Steel Research, 88(9), 134–149, 2013, doi: 10.1016/J.JCSR.2013.05.003.
[28] Rice J.R., and Tracey D.M., "On the ductile enlargement of voids in triaxial stress fields," Journal of the Mechanics and Physics of Solids, 17(3), 201-2017, 1969, doi: 10.1016/0022-5096(69)90033-7
[29] Eurocode 2, Design of concrete structures - Part 1-1: General rules and rules for buildings. London, 2002.
[30] Ellobody E., Young B., and Lam D., "Behaviour of normal and high strength concrete-filled compact steel tube circular stub columns," Journal of Constructional Steel Research, 62(7), 706–715, 2006. doi: 10.1016/J.JCSR.2005.11.002.
[31] Wang T. and Hsu T.T.C., "Nonlinear finite element analysis of concrete structures using new constitutive models," Computers & Structures, 79(32), 2781–2791, 2001. doi: 10.1016/S0045-7949(01)00157-2.
[32] GB50017-2003, Code for design of steel structure. Beijing, 2003.
[33] AISC, ANSI/AISC 360-05 specification for structural steel buildings. Chicago, Illinois, 2005.
[34] JSCE, Committee of steel structure: Standard specifications for steel and composite structures (Design edition). Tokyo, Japan, 2007.